FORMATION OF A FALLING PARTICLE CURTAIN

PETER VOROBIEFF[1], PATRICK WAYNE[1], SUMANTH REDDY LINGAMPALLY[1], GREGORY VIGIL[1], JOSH LUDWIGSEN[1], DANIEL FREELONG[1], C. RANDALL TRUMAN[1], & GUSTAAF JACOBS[2]
[1] Department of Mechanical Engineering, The University of New Mexico, Albuquerque, USA.
[2] Department of Aerospace Engineering, San Diego State University, USA.

ABSTRACT

Falling particle curtains are important in many engineering applications, including receivers for concentrating solar power facilities. During the formation of such a curtain, we observe a multiphase analog of Rayleigh–Taylor instability (RTI). It was originally described in 2011 for a situation when air sparsely seeded with glycol droplets was placed above a volume of unseeded air, producing an unstably stratified average density distribution that was characterized by an effective Atwood number 0.03. In that case, the evolution of the instability was indistinguishable from single-phase RTI with the same Atwood number, as the presence of the droplets largely acted as an additional contribution to the mean density of the gaseous medium. Here, we present experiments where the volume (and mass) fraction of the seeding particles in gas is considerably higher, and the gravity-driven flow is dominated by the particle movement. In this case, the evolution of the observed instability appears significantly different.
Keywords: experiment, hydrodynamic instabilities, multiphase flow, Rayleigh–Taylor instability.

1 INTRODUCTION

In classical hydrodynamics, several important instabilities can be described using the same idealized formulation [1]. Consider an inviscid, incompressible two-dimensional flow with a density interface in the $x - y$ plane near $y = 0$ separating fluids characterized by densities ρ_1 in the lower and ρ_2 in the upper half-plane. If the y-velocity is initially uniformly zero, and the uniform x-velocities U_1 (lower half-plane) and U_2 (upper half-plane) are not equal, the case of $\rho_1 = \rho_2$ will produce pure Kelvin–Kelmholtz instability (KHI). If both fluids are initially at rest, with $\rho_2 > \rho_1$, and are subject to constant acceleration g directed down the y axis, Rayleigh–Taylor instability (RTI) will develop, amplifying any interfacial perturbations. Finally, in the case when sustained acceleration is replaced with an impulsive acceleration (either in the positive or in the negative y-direction), Richtmyer–Meshkov instability (RMI) will manifest [2], [3]. KHI, RTI, and RMI play an important role in a wide variety of liquid, gas, and plasma flows and have been extensively studied. For RTI and RMI, the necessary condition for the instability is $\rho_1 \neq \rho_2$ on the interface. The dimensionless parameter essential for the characterization of both RMI and RTI is the Atwood number

$$A = \frac{\rho_2 - \rho_1}{\rho_2 + \rho_1} \tag{1}$$

Now consider multiphase flow where the embedding phase (gas or liquid) has a constant density, but the embedded phase (particles, droplets, etc.) is distributed non-uniformly, leading to the existence of gradients of average density. Recently, it was demonstrated [4]–[6] that analogues of RMI and RTI exist in such flows subjected either to gravity or to impulsive (shock) acceleration. The analogue of RMI [4] is known as shock-driven multiphase instability (SDMI) [6], [7]. As in the case of classical RMI, a dimensionless number similar to the Atwood number (eqn (1)) plays a key role in SDMI: the multiphase Atwood number [8]

ISSN: 2046-0546 (paper format), ISSN: 2046-0554 (online), http://www.witpress.com/journals
DOI: 10.2495/CMEM-V8-N1-27-35

$$A_m = \frac{\rho_s - \rho_u}{\rho_s + \rho_u} \tag{2}$$

Here, the subscript s characterizes the volume-averaged properties of the *seeded* flow (embedding phase together with embedded phase), and the subscript u the properties of the *unseeded* embedding phase.

Two limit cases can be considered: $A_m \to 0$ and $A_m \to 1$. Presently, the former case is somewhat better studied [4], [8]–[10], with investigations mostly focusing on SDMI. For $A_m \to 0$, gaseous embedding phase, and liquid or solid embedded phase (small micron or submicron-sized droplets or particles), it was shown that the SDMI growth can be (at least in first order) approximated with expressions originally derived for RMI, replacing A (eqn (1)) with A_m (eqn. (2)) [4]. Likewise, in this case shock-accelerated multiphase flow can be modeled (credibly but not perfectly) with models developed for the single-phase variable-density case (RMI) [11]. Differences between SDMI and RMI are nevertheless considerable: while shock-induced RMI is baroclinically driven (vortex formation is precipitated by misalignment between density and pressure gradients), in SDMI, vortex formation is driven by shear (similar to KHI), while shear is produced by massive particles or droplets interacting with the surrounding shock-accelerated gas and slowing it down.

One earlier study was also conducted for the multiphase analogue of RTI [5] for $A_m \sim 0.03$. For the flow under investigation (air with a small volume fraction of micron-sized glycol droplets), it was concluded that morphologically and in terms of instability growth, the results were indistinguishable from classical single-phase RTI, with droplet seeding effectively contributing only to local average density.

But what happens for the other limit case ($A_m \to 1$)? For the studies summarized in the preceding paragraphs, the flow was dominated by hydrodynamic effects. As A_m increases, particle interactions, particle inertia, etc. begin to play a more prominent role. In the following sections, we describe an experiment where a falling particle curtain forms with particle seeding density leading to $A_m \approx 0.98$. During the formation of this curtain, perturbations on its leading edge grow, similarly to what happens with an RTI-unstable interface. However, the growth rate appears very different from what is observed for classical RTI, and this can be explained by profound differences in the physics of the corresponding flows.

2 EXPERIMENTAL SETUP

The motivation for particle-curtain studies described here was twofold. First, we wanted to produce an average density interface characterized by a sufficiently high A_m for studies of its evolution under shock acceleration. Second, we were conducting a study on a related subject, operation of a falling particle curtain receiver used to store heat produced by a concentrating solar power facility [12]. Both the formation and the steady-state condition of the curtain proved much more interesting than anticipated.

Figure 1 shows the schematic (top) and the actual view of the experimental arrangement. In the top view, the particle–curtain setup is shown mounted on the UNM shock tube, which is described in detail elsewhere [8]. The arrangement is comprised of a modular extruded-metal frame used to mount the components, the horizontal element of which is the hopper rail. To the hopper rail, we attach the particle hopper. At the bottom of the hopper, a sliding plate is placed to keep the particles in prior to the beginning of the experiment. The same element serves to mount an electric motor that provides a small-amplitude vibration to the hopper. These components are vibration-isolated from the rest of the setup, the latter

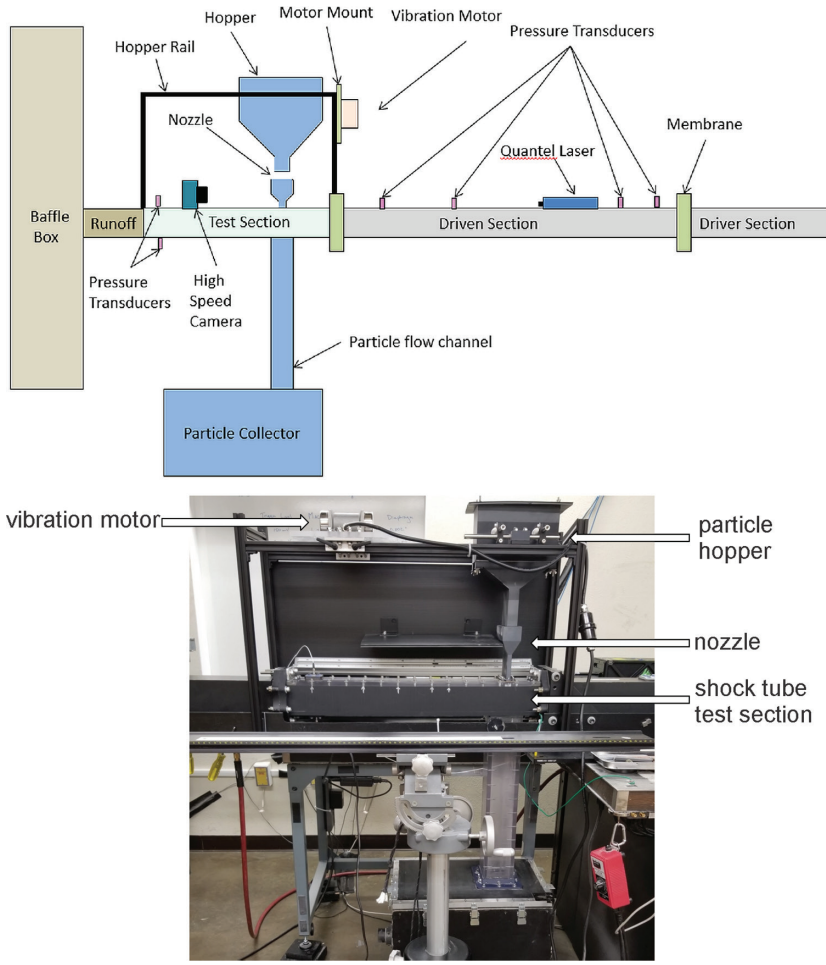

Figure 1: Top: schematic of the side view of the experimental arrangement, including the UNM shock tube and the particle-curtain setup. Bottom: close-up photo of the test section of the shock tube, the hopper rail, and the particle-curtain setup.

including the particle curtain-forming nozzle attached directly to the test section of the shock tube. In the experiments described here, the horizontal dimensions of the nozzle opening were 72×2 mm.

In the experiments described below, a typical run proceeded as follows. The hopper (sliding plate closed) was loaded with soda lime particles. The nominal particle diameter ranged between 30 and 50 μm, and the particle density was 1.44 g/cc. Then the vibration motor was turned on, and the sliding plate removed from the bottom of the hopper, releasing the particles into the nozzle below, then into the test section, then into the particle flow channel, and into the particle collector, from which the particles could be extracted for reuse. For experiments with shocked curtain, the location of the camera visualizing the curtain must be chosen outside the shock tube, as shown in Fig. 1, top, however, in the data presented here, the runoff

section of the setup connecting the test section of the shock tube with the baffle box was removed, making it possible to visualize the falling curtain so that the optical axis of the camera lens was at 90° to the plane of the curtain.

A Sony RX IV camera was used to capture images at 960 frames per second in full HD resolution. The camera was turned on shortly prior to the opening of the sliding plate, with data acquisition runs limited to 2 s by hardware. The curtain was illuminated through the transparent sides of the test section with two LED panels.

3 OBSERVATIONS AND ANALYSIS

Figure 2 shows (in false color) a sequence of four cropped images tracking the leading edge of the falling curtain. It takes about 60 ms for the edge of the curtain to reach the bottom of the test section and disappear into the particle flow channel. It is important to note that the distance between the bottom of the hopper with the sliding plate and the point where the particle curtain becomes visible is about 12 cm, so the particles are entering the field of view of the camera some time (about 200 ms) after the sliding plate is opened, giving any interfacial perturbations some time to develop. Another important aspect of the observed flow evolution that must be mentioned is that the centerline of the curtain edge in the vertical direction moves downward and accelerates. This necessitates a deviation from the way interfacial perturbations are usually measured in classical RTI studies, where after gravity-driven instability growth commences, bubbles of lighter gas or fluid go up, and spikes of heavier gas or fluid go down, and local instability amplitude can be measured in a stationary reference frame, from top of bubble to bottom of adjacent spike. Here, we have to track the leading

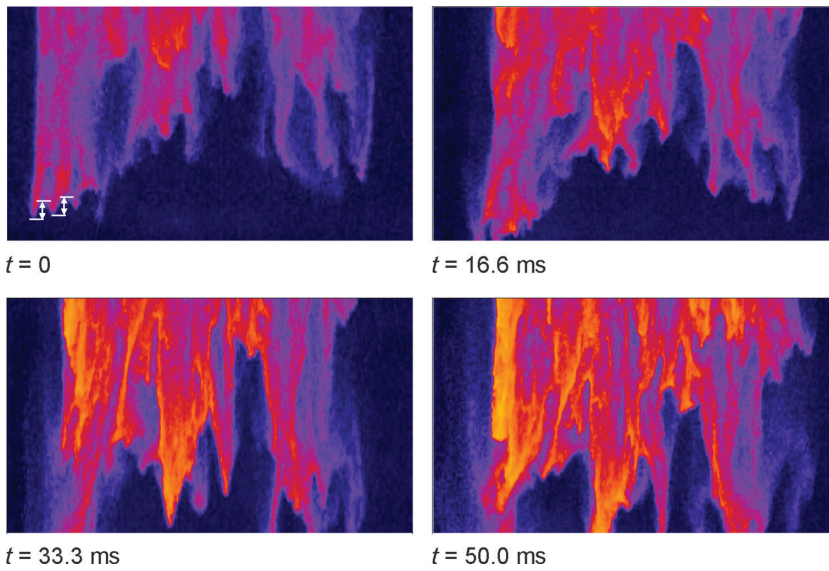

Figure 2: Four images (false-color) tracking the leading edge of the falling particle curtain. Time $t = 0$ corresponds to the moment the leading edge of the curtain clears the nozzle and becomes fully visible in the test section. The width of the field of view is 76 mm. Arrows in the first image show two examples of perturbation amplitude measurements.

edge of the curtain, and make the same measurements (perturbation amplitude bubble-to-spike) in a moving reference frame.

With these caveats, it is still apparent that the leading edge of the curtain is perturbed, and the perturbation is growing.

Three data sequences with identical initial conditions were acquired and analyzed to measure peak-to-peak amplitudes at seven timings, from 0 to 50 ms after the falling curtain enters the field of view of the camera. From each sequence, a single frame at seven timings (0, 8.3, 16.6, 24.9, 33.3, 41.6, and 50 ms) was analyzed, yielding up to 12 bubble-to-spike amplitude measurements. Figure 3 shows the analysis results. Both the images and the plot show considerable variance in the perturbation amplitude, but the overall trend in perturbation growth with time is quite close to linear: the coefficient of determination $r^2 = 0.97$ for the fit shown in the plot.

Additional characterization of the curtain in terms of velocity field and mass flow rate was also undertaken [13]. The mass flow rate was measured directly, by monitoring the initial and transient weight of the particle collector (44.16, 0.12 g/s). Velocity-field measurements of a curtain that reached steady-state [14] reveal that the average vertical velocity grows linearly with downstream distance (and thus with time). With the known average velocity and mass flow rate, the volume fraction of the particles can also be found from simple conservation-of-mass considerations. For the steady-state curtain, it varied from 8.4% at the top of the test section to 2.5% at the bottom. In terms of the multiphase Atwood number (eqn (2)), this translates to $0.98 > A_m > 0.95$. The curtain is indeed in the $A_m \rightarrow 1$ regime.

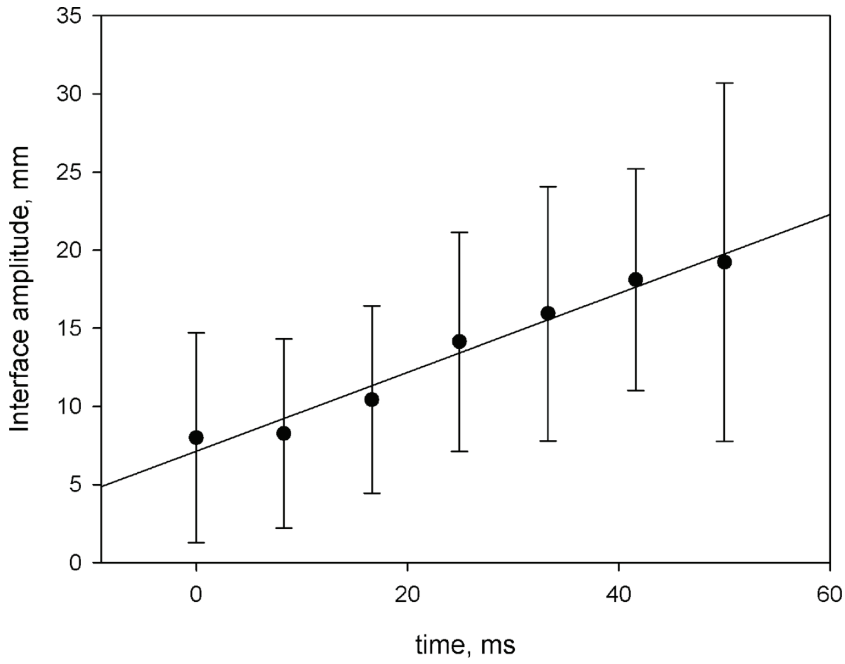

Figure 3: Time history of the perturbation amplitude on the leading edge of the falling curtain. Error bars show the standard deviation at each timing. Straight line: linear fit.

What can account for the stark difference between the interfacial perturbation evolution in classical RTI (quadratic) and what we observe for the falling particle curtain? Two explanations are possible. One possibility is that the observation window used in our experiment is insufficient to track the quadratic growth. The other possibility is that the growth is both dominated by physics somewhat different from the classical RTI and observed in a different (accelerating) reference frame. Based on both mass-conservation considerations and direct measurements [13], as the curtain accelerates downward, its local particle seeding concentration decreases, leading to a small but noticeable and highly repeatable decrease in A_m. Now consider the classical quadratic-growth instability amplitude h growth formula for RTI

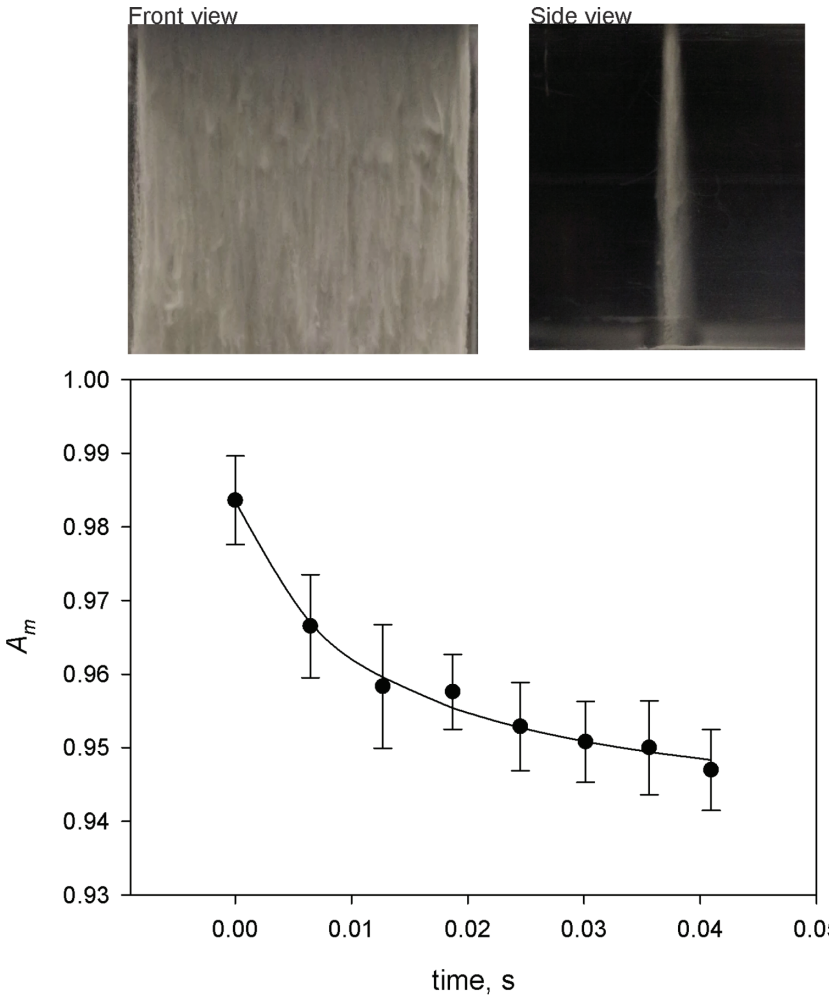

Figure 4: Top: front and side images of the falling curtain showing the entire field of view, top to bottom. Bottom: Multiphase Atwood number in the curtain as a function of time. Time $t = 0$ corresponds to the moment when the flow enters the field of view at the top of the test section. The line is the best fit to the data using eqn (3) with parameters described in the text.

$$h = \alpha A g t^2$$

where α is a constant (on the order of 0.05). Now let us replace A with A_m slowly (at a rate ε) decreasing in time to an equilibrium terminal-velocity value $A_{m,t.v.}$, with a time offset t_e (time to account for curtain development as it leaves the nozzle)

$$A_m = \frac{\varepsilon}{t + t_\mu} + A_{m,t.v.} \tag{3}$$

Then let us transition into a reference frame accelerating at a rate

$$h_{m,t.v.} = \alpha A_{m,t.v.} g t^2$$

This reference frame to first order will correspond to the frame following the falling-curtain edge, and the perturbation growth in that frame will be

$$\partial h = a \frac{\varepsilon}{t + t_e} g t^2$$

For sufficiently late t, $t \gg t_e$, and δh ~ t, manifesting linear growth.

For a more realistic consideration, local particle seeding density variability, leading to local fluctuations of A_m, should be taken into account, as it likely produces the velocity differences along the edge of the falling curtain. The relevant physics at $A_m \to 1$ are dominated by particle inertia, unlike $A_m \to 0$ or classical RTI. For $A_m \to 1$, the baroclinic vorticity production mechanism in fluid (vorticity generation proportional to the cross-product of density and pressure gradients) is less relevant, and the most likely key hydrodynamic characteristic is the local terminal velocity of a particle-seeded volume, which would vary with A_m.

Figure 4 shows front and side snapshots of the curtain over the entire 7.6 cm vertical extent of the test section, and the plot of the time evolution of A_m based on the data collected earlier [13], [14] for the average velocity and mass-discharge rate of a curtain that achieved a steady state. The fit to the data uses eqn (3), with the parameters as follows: $\varepsilon = 4.9 \times 10^{-4}$, $t_e = 0.011$, $A_{m,t.v.} = 0.939$, time in s. The coefficient of determination for this best fit is $r^2 = 0.991$. Note that these values are largely consistent with the assumptions we made above regarding the order of magnitude of the parameters: $\varepsilon \ll 1$, $t_e \ll t$, and $A_{m,t.v.} \sim 1$.

4 CONCLUSIONS

Similar to SDMI, a multiphase gravity-driven instability (MGDI) also appears to exist. As SDMI can be regarded as a multiphase analogue of RMI, so the MGDI corresponds to RTI. Two limit cases exist for MGDI. In terms of multiphase Atwood number A_m, the first limit case is $A_m \ll 1$. For this case, behavior similar to RTI was observed, with flow dominated by hydrodynamic effects, and the embedded phase following the flow. We show the second case, $A_m \to 1$, to manifest behaviors distinct from RTI. The $A_m \to 1$ flow is likely to be dominated by particle effects, although fluid mechanics still must play a role. We observe linear growth of perturbations along the leading edge of the curtain and offer a simple explanation based on the flow phenomenology and theory for the linear trend, which is distinct from quadratic growth for classical RTI and consistent with earlier experiment.

Future studies are required to elucidate some features observed in the $A_m \to 1$ falling-curtain flow. Flow visualization shows persistent formation of perturbations with features at similar wavelengths (Fig. 2). The wavelength selection mechanism is presently unclear. A longer observation interval will help determine how long the linear perturbation amplitude growth

persists. It would also be very instructive to study the same falling-curtain formation in vacuum, to determine the actual contribution of hydrodynamic effects. The parameter range for A_m should also be extended through the entirety of the possible values ($0 < A_m < 1$): now we know something about the limit cases (very high and very low values), but a very important special case remains to be studied: flow with both gaseous density gradients ($A \neq 0$) and seeding ($A_m \neq 0$) where neither feature is clearly dominant.

We also seek to understand growth rates by conducting numerical analysis using an approach similar to the Eulerian–Lagrangian study of the particle-laden RMI [6].

ACKNOWLEDGEMENTS

This work is supported by the US National Science Foundation (NSF) grant 1603915. We also acknowledge partial support from the US Defense Threat Reduction Agency (DTRA) grant HDTRA1-18-1-002 and National Nuclear Security Administration (NNSA) grant DE- NA-0002913.

We also owe special thanks to Xylar Asay-Davis for developing the ACCIV (advection-corrected correlation image velocimetry) code [15] we used to quantify the falling curtain velocity [14].

REFERENCES

[1] Currie, I.G., *Fundamental Mechanics of Fluids*, CRC Press; 2002.

[2] Richtmyer, R.D., Taylor instability in shock acceleration of compressible fluids. *Communications on Pure and Applied Mathematics*, **13(2)**, pp. 297–319, May 1960. https://doi.org/10.1002/cpa.3160130207

[3] Meshkov, E.E., Instability of the interface of two gases accelerated by a shock wave. *Fluid Dynamics*, **4(5)**, pp. 101–104, 1 September 1972. https://doi.org/10.1007/bf01015969

[4] Vorobieff, P., Anderson, M., Conroy, J., White, R., Truman, C.R. & Kumar, S., Vortex formation in a shock-accelerated gas induced by particle seeding. *Physical Review Letters*, **106(18)**, p. 184503, 4 May 2011. https://doi.org/10.1103/physrevlett.106.184503

[5] Vorobieff, P., Anderson, M., Conroy, J., White, R., Truman, C.R. & Kumar, S., Analogues of Rayleigh-Taylor and Richtmyer-Meshkov instabilities in flows with nonuniform particle and droplet seeding. *WIT Transactions on Engineering Sciences*, pp. 17–28, 27 May 2011. https://doi.org/10.2495/mpf110021

[6] Gonzalez Izard, R., Lingampally, S.R., Wayne, P., Jacobs, G. & Vorobieff, P., Instabilities in a shock interaction with a perturbed curtain of particles. *International Journal of Computational Methods and Experimental Measurements*, **6(1)**, pp. 59–70, 2017. https://doi.org/10.2495/cmem-v6-n1-59-70

[7] Frost, D.L., Heterogeneous/particle-laden blast waves. *Shock Waves*, **28(3)**, pp. 439–449, May 2018. https://doi.org/10.1007/s00193-018-0825-1

[8] Anderson, M., Vorobieff, P., Truman, C.R., Corbin, C., Kuehner, G., Wayne, P., Conroy, J., White, R. & Kumar, S., An experimental and numerical study of shock interaction with a gas column seeded with droplets. *Shock Waves*, **25(2)**, pp. 107–125, 2015. https://doi.org/10.1007/s00193-015-0555-6

[9] McFarland, J.A., Black, W.J., Dahal, J. & Morgan, B.E., Computational study of the shock driven instability of a multiphase particle-gas system. *Physics of Fluids*, **28(2)**, p. 024105, 2016. https://doi.org/10.1063/1.4941131

[10] Black, W.J., Denissen, N.A. & McFarland, J.A., Evaporation effects in shock-driven multiphase instabilities. *Journal of Fluids Engineering*, **139(7)**, p. 071204, 2017.
[11] Anderson, M., Vorobieff, P., Kumar, S., Conroy, J., White, R., Needham, C. & Truman, C.R., Numerical simulation of a shock-accelerated multiphase fluid interface. *In* 28*th International Symposium on Shock Waves*, Springer, Berlin, Heidelberg, pp. 923–929, 2012.
[12] Ho, C.K., Kinahan, S., Ortega, J.D., Vorobieff, P., Mammoli, A. & Martins, V., Characterization of particle and heat losses from falling particle receivers. *In Proceedings of the ASME 2019 13th International Conference on Energy Sustainability*, pp. 1–10.
[13] Freelong, D., Reflections of a shock wave off a sparse curtain of particles. *Presented at* 2019 *AIAA Region IV Student Conference*, pp. 29–31, March 2019.
[14] Vigil, G., Vorobieff, P., Freelong, D., Wayne, P. & Truman, C.R., Validating advection-corrected correlation image velocimetry. *Bulletin of the American Physical Society*, **63(13)**, p. 613, 2018.
[15] Asay-Davis, X.S., Marcus, P.S., Wong, M.H. & de Pater, I., Changes in Jupiters zonal velocity between 1979 and 2008. *Icarus*, **211(2)**, pp. 1215–1232, 2011. https://doi.org/10.1016/j.icarus.2010.11.018